Phospholipid Monolayer/Graphene Interfaces: Curvature Effect on Lipid Morphology and Dynamics

Mohan Teja Dronadula and N. R. Aluru*

Oden Institute for Computational Engineering and Sciences Walker Department of Mechanical Engineering The University of Texas at Austin, Austin, Texas 78712

ABSTRACT

Phospholipids are an important class of lipids that are widely used as model platforms for the study of biological processes and interactions. These lipids can form stable interfaces with solid substrates, such as graphene, and these interfaces have potential applications in biosensing and targeted drug delivery. In this paper, we perform molecular dynamics simulations of graphene-supported lipid monolayers to characterize the lipid properties of such interfaces. We observed substantial differences between the supported monolayer and free-standing bilayer in terms of the lipid properties, such as the tail order parameters, density profiles, diffusion rates, etc. Furthermore, we studied these interfaces on sinusoidally deformed graphene substrates to understand the effect of curvature on the supported lipids. Here, we observed that the nature of substrate curvature, i.e., concave or convex, can locally affect the lipid/substrate adhesion strength and induce structural and dynamic changes in the adsorbed lipid monolayer. Together, these results help characterize the properties of lipid/graphene interfaces and provide insights into the substrate curvature effect on these interfaces, which can enable the tuning of lipid properties for various sensor devices and drug delivery applications.

KEYWORDS: molecular dynamics, phospholipids, graphene, supported lipid monolayers, biosensors, soft matter.

^{*} Corresponding Author, e-mail: <u>aluru@utexas.edu</u>, web: <u>https://sites.utexas.edu/aluru/</u>

INTRODUCTION

The unique properties of cell membranes allow them to play a crucial role in the survival of cells. Apart from maintaining the cell structure, they act as semipermeable membranes to selectively allow molecules to diffuse through¹, host transmembrane proteins, which is important for the transport of materials in and out of cells² and play an important role in cell signaling and communication³. Hence, it is important to study and understand the various processes that occur in cell membranes. Lipid bilayers are the major constituents of cell membranes, and they are constructed in vitro to serve as simplified models to study the various physical and chemical properties of cell membranes^{4–6}. There are various techniques for constructing and studying these model membranes. For example, thin lipid bilayers have been traditionally formed across an aperture in the aqueous phase to study the electrochemical properties of cell membranes^{7–9}. These lipids, termed black lipids, are unstable, thereby preventing their use in studies of long-term processes 10,11. Hence, in recent decades, several studies on long-term membrane processes have formed stable structures using supported lipid structures, such as supported lipid bilayers (SLBs), supported lipid monolayers (SLMs), and tethered bilayer lipid membranes (t-BLMs)^{11–14}. Apart from offering higher stability, SLBs have also made it possible to use a range of characterization techniques, such as atomic force microscopy (AFM)¹⁵, secondary ion mass spectrometry (SIMS)¹⁶, and scanning probe microscopy¹⁷, which is not possible with freely floating lipid bilayers.

In the past decade, supported lipid systems have also been applied for protein crystallization¹⁸, biosensing^{19–21}, targeted drug delivery system design^{22,23}, etc. Two-dimensional (2D) materials, such as graphene, graphene oxide (GO) and reduced graphene oxide (r-GO) interfaced with lipid monolayers and bilayers, have been successfully used to construct highly sensitive, label-free biosensing apparatuses. The high sensitivity of graphene to electronic changes in the surrounding

environment was used to study various membrane-protein interactions, detect the presence of toxins, etc. 20,21,24-26.

Although supported lipids have been used successfully for various applications, very few studies have focused on the effect of substrates on the properties of lipids in these interfaces. Studies have reported the effect of substrates in SLBs and SLMs^{27–30}, although an extensive characterization of the structure and dynamics of lipids, especially in SLMs (where there is direct contact between the substrate and lipids), is lacking. However, the changes in lipid properties in these interfaces can directly affect the behavior and performance of supported lipids in various applications; hence, it is important to characterize and understand them.

Another important aspect of these interfaces is substrate deformation. Static and dynamic wrinkles may be inherently present in 2D materials depending on the method of preparation^{31,32}. Deformations may also be deliberately incorporated to change the electronic properties of the substrate to enhance sensing capabilities. For example, in a recent study, it was shown that using a deformed sheet of graphene instead of a flat sheet in graphene-based FETs enhances the sensing capabilities of the device. The resultant apparatus was able to sense DNA at attomolar concentrations³³. Moreover, in drug delivery applications, the substrate curvature can be used to achieve specific functionality; for example, a recent study used gold nanoparticles of a specific shape coated with lipids to deliver DTX selectively to cancerous cells²².

The presence of substrate curvature, whether induced or inherently present, can locally affect the morphological and dynamical properties of the supported lipids. To our knowledge, previous studies have not reported the nanoscale effects of substrate curvature on the properties of supported lipids, especially SLMs. However, understanding the substrate and curvature effects on supported lipid interfaces can be invaluable in designing better apparatus for sensing and drug delivery

applications. Hence, in the present study, using molecular dynamics and coarse-grained molecular dynamics simulations, we characterize the effects of the presence of substrate and curvature on a graphene-supported monolayer of 1,2-dioleoyl-sn-glycero-3-phosphocholine (DOPC) lipids.

METHODS

Lipid bilayer simulations- In this study, DOPC lipid bilayer systems were simulated to serve as systems without a substrate. The structural properties, such as the tail order parameter, density profile and tail tilt angle distribution, and a dynamical property, specifically, the lateral diffusion coefficient, were computed for the free-standing bilayer systems and compared with those of the flat and deformed graphene-supported systems. The computed results provide information on how the substrate's presence affects the lipid tails (see the results and discussion sections). A 252 DOPC lipid bilayer system (126 lipids per monolayer) with full hydration (50 water molecules per lipid) was simulated for 250 ns using the all-atom empirical CHARMM36m force field³⁴. The system was simulated in an NPT ensemble at 300 K and 1 atm pressure. Temperature was controlled using the modified Verlet algorithm to solve the Langevin equation^{35,36}. The pressure was controlled using the modified Nosé-Hoover method with Langevin dynamics controlling the piston fluctuations 37,38 . The membrane lateral (x-y) and perpendicular (z) directions were separately coupled to the barostat to ensure a zero surface tension value. The long-range electrostatics were computed using the PME method³⁹. The simulation was performed using the NAMD⁴⁰ molecular simulation package with the TIP3P water model⁴¹. A snapshot of the simulation system is shown in Figure 1(a), and the visualization was performed using the VMD⁴² package. An initial 200 ns of simulation was performed to ensure that the system reached equilibrium. An additional 50 ns simulation was performed to compute the bilayer properties.

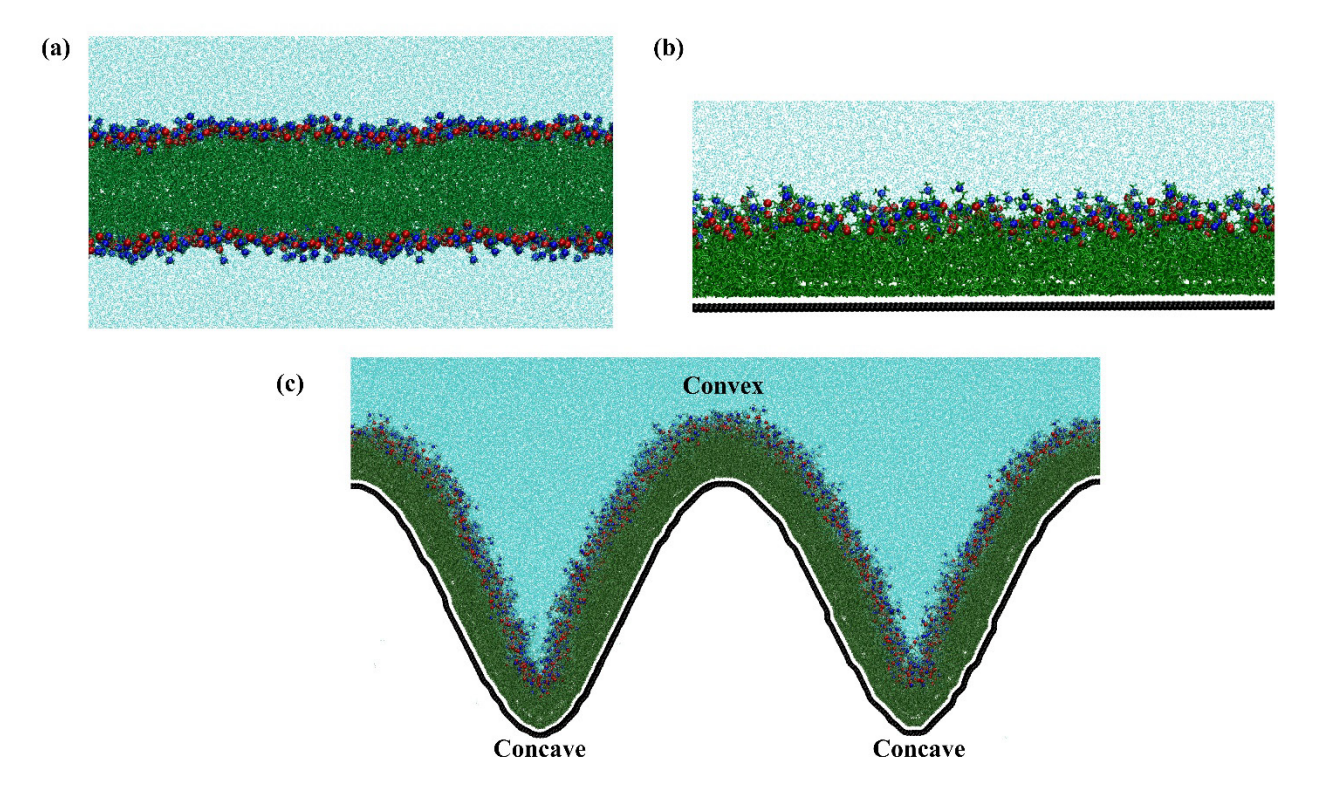


Figure 1 Visualization of the simulated systems (a) 126 x 126 DOPC bilayer, (b) 126 DOPC SLM on a flat graphene (black spheres) substrate, (c) 2231 DOPC lipid SLM on a sinusoidally crumpled graphene substrate.

SLM simulations- In this study, SLM simulations were performed using graphene as the substrate. The choice of this substrate can be justified by its extensive applications in biosensing and strong lipophilic characteristics, which help stabilize the lipid monolayer. Two different kinds of supported systems were considered in this study: a flat graphene SLM and a deformed graphene SLM. Simulations were performed in the NVT ensemble at 300 K. The simulation setups for both flat and crumpled graphene cases consisted of a lipid monolayer adsorbed onto a graphene substrate (along the z-direction) through direct adsorption and onto a water layer above the lipid monolayers to stabilize it. A vacuum layer was implemented above the water box to avoid

graphene-water interactions, and care was taken to ensure that the water reached the bulk water density at the water-vacuum interface. The simulation systems are shown in Figures 1 (b) & (c).

For the deformed graphene system, a sinusoidally curved (uniaxially along the x-direction) sheet of graphene with wavelength (λ) = 15 nm and amplitude (A) = 5 nm was used. The crumpled graphene was generated by adsorbing a large flat graphene sheet onto a silicon (Si) substrate, which was cut into the required sinusoidal shape (see the supporting information for more details). The concave and convex regions (see Figure 1 (c)) of the crumpled supported systems were analyzed separately to understand the effects of the nature of substrate curvature on the properties of supported lipids.

A DOPC monolayer composed of 126 lipids (taken from a pre-equilibrated bilayer) was adsorbed onto a 9.3 x 9.3 nm² flat sheet of graphene. The graphene was generated in *x-y* plane using the VMD package. It should be noted that the experimental packing density of lipids on a substrate could be different from their packing density in a bilayer. However, to facilitate a direct comparison with lipids in a bilayer (removing the effects of packing), we set the area of the graphene sheet equal to the average equilibrium area of the 126x126 lipid bilayer. This choice can be further justified by previous experimental studies^{43,44} where the area of the membrane was controlled in graphene and graphene-oxide SLMs, using the Langmuir-Blodgett technique⁴⁵. It should however be noted that, this choice could result in negative lateral pressures^{46,47}, which may affect the properties computed in this study. However, the objective of this study is to compare the properties of SLMs for different substrate curvatures when the packing of lipids is controlled rather than tension.

For the deformed graphene case, initially, the lipids were packed to the same density as the flat case, although the deformed graphene was unable to accommodate the same packing density.

Some lipids detached from the substrate and monolayer, entered the water layer, and eventually floated to the water-vacuum interface. Hence, the overall lipid packing is slightly lower in the deformed case and changes with the curvature. However, the reduction in packing was very less and its effect on the properties of lipids (in the flat part of the curved SLM system) was insignificant.

A 250 ns long simulation was performed for the flat case, with the last 50 ns used for computing the lipid properties. In the crumpled case, due to the large system size, a 170 ns simulation was performed, with the last 30 ns used for analysis. Care was taken to ensure that the computed properties converged properly. Simulations were performed using the CHARMM36m force field implemented in the NAMD molecular simulation package.

Order-parameter- The deuterium tail order-parameter gives a measure of the order in the lipid tails. These order parameters obtained through nuclear magnetic resonance (NMR) are often used to quantify the accuracy and calibrate molecular force fields⁴⁸. The order-parameter is computed as follows:

$$S_{C-H} = \frac{1}{2}(3\cos^2(\theta) - 1) \tag{1}$$

where S_{C-H} is the carbon-hydrogen acyl chain order-parameter and "Θ" is the angle made by the carbon hydrogen (C-H) bond with the bilayer normal, as shown in Figure 2 (d). S_{C-H} is computed for every carbon in the lipid tails "sn1" (first tail) and "sn2" (second tail). A comparison of the order-parameter plots (-S_{C-H} vs carbon number) for the various systems is reported in the results section (Figure 3). The order-parameter values range from "-0.5" (perfect order) to "1" (perfect order but with the tails oriented perpendicular to the bilayer or monolayer normal). A value of "0" indicates a disordered system. It should be noted that the order-parameter plots reported in the results section represent the -S_{C-H} vs carbon number, which is the most conventional representation in the literature. Negative values of -S_{C-H} are observed only in the supported lipid cases because the lipid tails bend to increase the adsorption area²⁹.

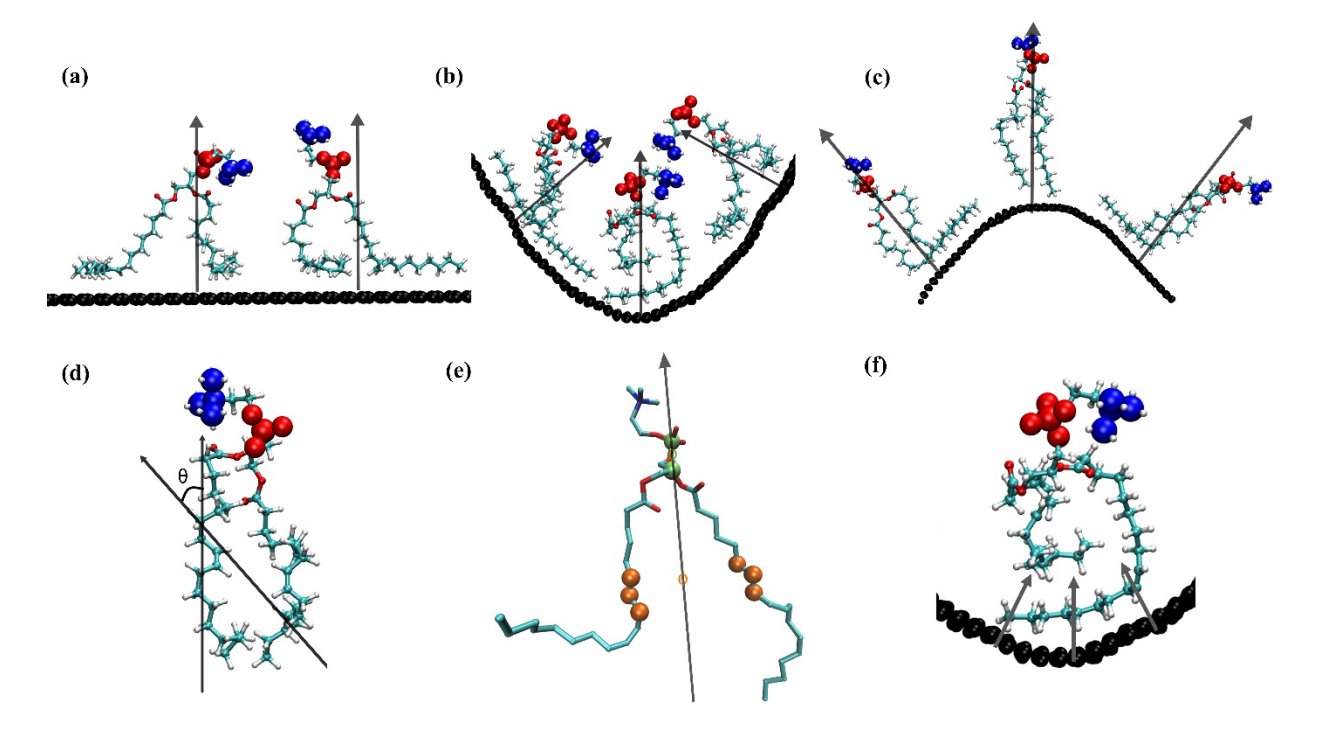


Figure 2 (a), (b) & (c) represent the orientation of lipids on flat, concave and convex graphene substrates, respectively, (d) representation of the angle (Θ) used for computing order-parameter, (e) representation of the molecular normal where the head groups and tail groups used for computing the center of masses are depicted by green and orange spheres respectively, (f) representation of the normals used for computing the order-parameter of proximal carbon atoms.

To better understand the effects of the substrate, the lipid tail carbon atoms were classified into proximal (closer to graphene) and distal (away from graphene) parts. Tail carbons away from the substrate and above the unsaturation (C9-C10 bond) are categorized as distal carbons, and the carbons closer to the substrate (below the unsaturation) are categorized as proximal carbons. The computation of the order parameter for lipids in a bilayer and supported monolayers on flat

substrates is rather straightforward and extensively done, both in computational and experimental studies. On the other hand, the computation of this property for lipids on a curved substrate is not directly evident because the lipid orientation becomes a changing local property (Figure 2 (a)(b)(c)).

To overcome this challenge, we adopted a molecular director approach similar to the one used in a previous study⁴⁹ for the carbons in the distal part (Figure 2 (e)). For each of the carbons in the proximal part where the substrate effects control the lipid behavior, the normal is defined as the unit vector pointing from the nearest graphene carbon to the lipid carbon (Figure 2 (f)). The order parameter helps us understand how the substrate affects the order and conformational stability in lipid tails. The results section discusses that in detail, specifically the effect of substrate and curvature on the tail order of the supported lipids.

Tilt angle distributions- The tilt angle distribution provides a direct measure of the extent of tail tilt or bending in the lipids and is computed as the angle between the monolayer normal (+z direction except for the crumpled systems) and the vector connecting the first carbon and the last carbon of the lipid tails (Figure 4(a)). For the crumpled case, since the orientation of the lipids changes as a local property, we use the same molecular normal approach used for computing the order-parameter. The computed tilt angles of all the lipids were binned into equally spaced bins $(\Delta \theta = 1^{\circ})$ between 0° and 180° . The distributions from all the time frames were averaged to obtain the final distributions reported in the results section.

The tilt angle distributions helped to directly visualize the effect of the substrate on the lipid tails. The higher the influence, the higher the tilt in the lipid tails, which will cause the

distribution to shift to higher angles. These distributions also provided information on how the substrate curvature further affects tail bending.

Density profiles- Density profiles, such as mass density and electron density profiles, provide direct observations of the physical structure and distribution of a system. Moreover, density profiles can be used to study many of the important structural properties of lipids, such as the thickness, head and tail group distributions, and water penetration extent.

Here, we compute the mass density profiles of the lipid monolayers for the different systems considered. For the case of a lipid bilayer, the average center of the bilayer is taken as the reference. Binning is performed using a bin size of 0.5Å in the directions perpendicular to both monolayers (+z and -z directions), and the results are averaged over multiple time frames. In the flat graphene case, graphene acts as the reference point and binning is performed perpendicular to it (+z direction). In the case of deformed graphene (both concave and convex), binning is again performed perpendicular to the substrate, although this direction changes as a local property. The distance of each atom of the lipids to the closest carbon atom is binned in this case.

To facilitate comparisons, we divided the lipid molecules into head and tail groups. The carbon atoms C11-C15, nitrogen (N), phosphate (P), oxygen atoms O11-O14, and the associated hydrogen atoms were grouped under the head group category. The carbon atoms C23-C218, C33-C318 and associated hydrogen atoms were grouped under the tail group category (atoms names are as defined by the charm forcefield for lipids)

The density plots reported in the results section (Figure 5) provided information on how the presence of the substrate changes the thickness and distribution of the lipid head and tail groups (separate plots were generated to understand the differences in the substrate effect on head and tail groups). Further, the effect of substrate curvature was also clearly characterized in these density plots.

Coarse-grained simulations- In this study, we used the MARTINI v2.3p^{50–52} force field to simulate coarse-grained versions of the same all-atom systems. We implemented the force field in the GROMACS^{53–57} molecular simulation package, and a polarizable water model was used⁵⁸. We used the same ensembles and thermodynamic conditions as the all-atom systems (NPT for bilayer and NVT for supported systems). A velocity rescaling thermostat⁵⁹ was used to maintain the temperature, and a Parrinello-Rahman barostat⁶⁰ was used for pressure coupling. We computed the density profiles and tilt angle distributions using the coarse-grained trajectories to ensure that the force field can reproduce the trends observed in the all-atom systems (see the supporting information for the benchmarking results). Microsecond (μs) simulations were performed to compute the long-term diffusion coefficient of lipids. The methods for computing the density profiles and tilt angle distributions are the same except for the definition of the molecular normal (see Figure S2(g)).

Lipid lateral diffusion- The diffusion coefficient provides a measure of the lateral (x-y plane) mobility of the lipids in a bilayer or a monolayer and represents an important dynamic quantity because it directly controls the time scales of various membrane-bound phenomena, such as molecule diffusion⁶¹, phase separation, and lipid mixing⁶². Various factors can affect the lateral diffusion rate of lipids⁶³, such as the temperature, hydration, lateral packing density, and substrate

adhesion. Hence, it is important to study the effect of substrate and curvature on the local diffusion of supported lipids.

The diffusion coefficient is calculated as the slope of the mean square displacement (MSD) profile using Einstein's relation⁶⁴:

$$MSD(\tau) = 2dD\tau \tag{2}$$

$$MSD(\tau) = \langle (r(\tau) - r(0))^2 \rangle$$
 (3)

Here, "d" is the dimensionality of the system, "D" is the diffusion coefficient, " τ " is the lag time, $r(\tau)$ is the position, r(0) is the position for an arbitrarily chosen initial time, and <> denotes the ensemble average. The MSD profiles and the computed diffusion coefficients are reported in the results section.

In this study, 2-D (*x-y* directions) MSD (Figure 6(a, b)) and diffusion coefficients (Table 1) are reported for bilayer and flat supported cases, whereas 1-D (*y*-direction) MSD (Figure 6(c, d)) and diffusion coefficients are reported for the concave and convex crumpled cases to avoid inhomogeneities in the surface along the *x*-direction and ensure a fair comparison.

RESULTS & DISCUSSION

Order parameter- In this study, we computed and compared the acyl chain order parameter for the various supported cases considered to understand the effect of substrate and curvature on the lipid tail order. Additionally, we computed the order parameter for a lipid bilayer to compare with the supported cases. Figure 3 compares the order-parameter plots for the different substrate curvatures and the bilayer case. We differentiated the substrate curvatures into flat, concave, and convex, as explained in the methods section. The lipid tail carbon atoms have been differentiated into proximal (close to graphene) and distal (away from graphene) as explained in the methods section.

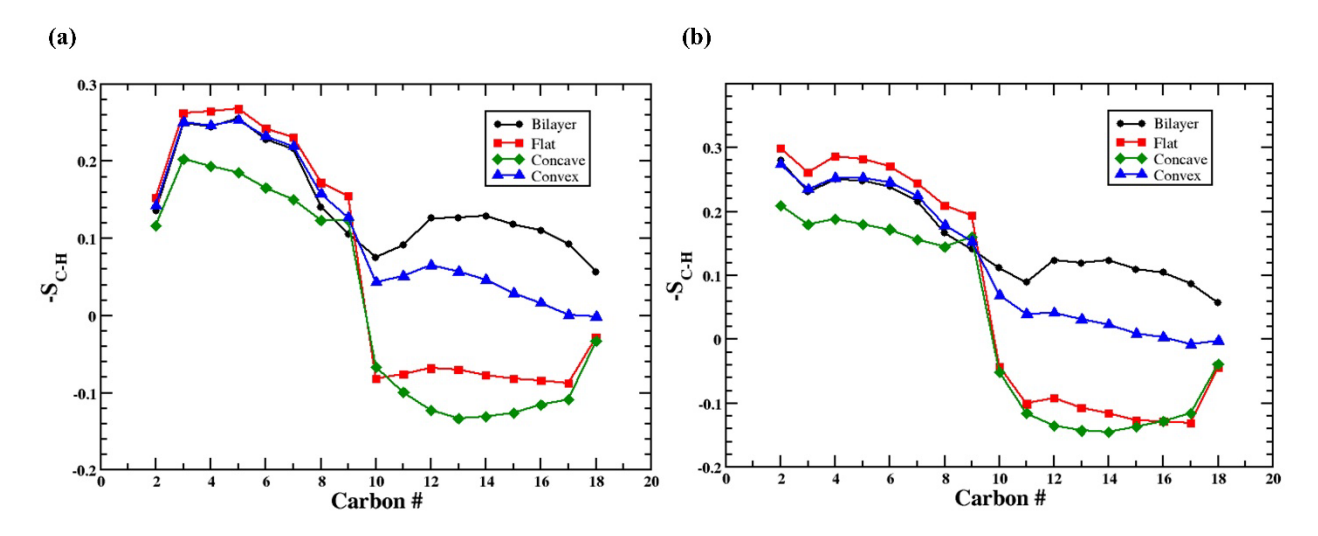


Figure 3 (a) comparison of the tail sn-1 order-parameter for the various systems, (b) comparison of the tail sn-2 order-parameter for the various systems.

Figure 3 shows that the distal parts of the lipids in the concave and convex regions are slightly less ordered than that of the lipids on a flat substrate, which was also previously observed in the case of curved bicelles⁶⁵. However, the proximal part of the lipids exhibited a different trend, with lipids in the concave region more ordered, followed by lipids on a flat substrate and lipids in the convex region. This observation can be explained in terms of the differences in the lipid

substrate interactions. The concave nature of the substrate enhances the lipophilic interactions between graphene and the lipid tails, whereas the opposite occurs in the convex region. It should be noted that the negative values of the order parameter observed for carbon atoms in the proximal part of the concave and flat cases are due to the bending of lipid tails, and a higher negative value indicates a higher order. We have directly computed the average interaction energies between the terminal tail carbon (C218) and graphene for the three cases. The interaction energy was the highest for concave (-4.174 \pm 0.13 KJ/mol), followed by flat (-2.46 \pm 0.137 KJ/mol) and convex (-1.671 \pm 0.07 KJ/mol) cases. It should be noted that the average distance of the C218 carbon atoms is similar for both the flat and concave cases (see Figure 5(c)). This indicates that the lipophilic characteristics of graphene can be enhanced or weakened by inducing curvature which directly affects the lipid tail order.

Furthermore, the average area-per-carbon values of graphene in the flat, concave and convex cases are 2.6121 Å², 2.60053 Å² and 2.6245 Å², respectively. There is only ~0.4% areal strain in the curved cases, compared to the flat case. Hence, the observed differences in the interaction energies are a result of the substrate curvature and membrane curvature, with negligible contribution from local strain.

Additionally, there is also a possibility of band gap opening due to crumpling. Some studies have shown that a bandgap can be opened by sinusoidally crumpling graphene⁶⁶, although the radius of curvature at the peaks and valleys of graphene used in those studies was quiet low. In another study⁶⁷, using a cylindrically deformed (not a CNT) graphene with radius of curvature "12.245 Å" (radius of curvature in this study is 11.4 Å at the peaks and valleys), it was shown that there was no band gap opening. While it is still possible that a bandgap could exist for the crumpled

graphene used in this study which may affect the substrate-lipid interactions, studying those effects is beyond the scope of this paper and will be studied in a future publication.

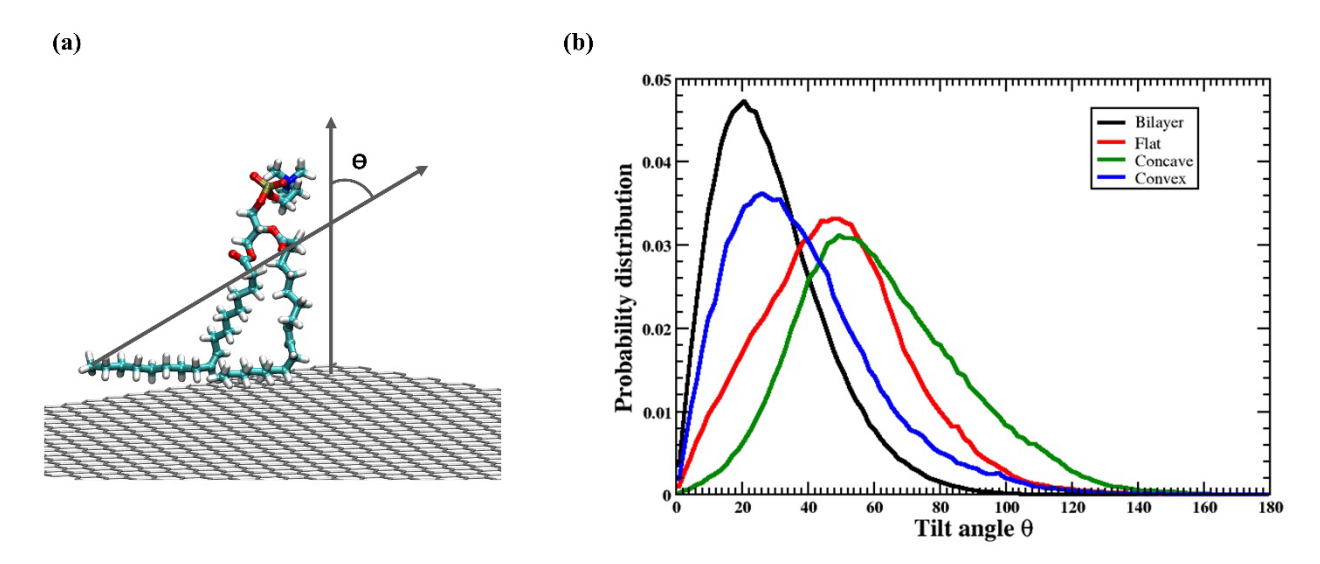


Figure 4 (a) Representation of the tilt angle (Θ) for a flat graphene supported lipid, (b) comparison of the tilt angle distributions for lipids in the various systems considered in this study.

Tail tilt-angle distributions- The order parameter tells us about the differences in the lipid tail order caused by the influence of substrate and curvature. It also shows that the proximal part of the lipid tails are bent in the supported cases, although it does not give a detailed understanding of the extent of bending in the lipid tails. To supplement our understanding of the local physical properties of the lipid tails, we computed the tilt angle profiles for lipids in each of the three systems as well as for the bilayer case.

Figure 4(b) compares the tilt angle distributions averaged over time for the four cases: bilayer, monolayer on flat graphene, monolayer on concavely curved graphene and monolayer on convexly curved graphene substrates. It should be noted that to facilitate direct comparison, we

used the same molecular director approach as we did for computing the order parameter (see methods section), thereby ensuring that the effect of the changing lipid orientations in the curved cases is removed.

The distributions showed that unlike the bilayer case, supported lipids exhibit a much wider distribution due to the bending of the lipid tails on a substrate, which results in an increase in the tilt angles. Within the supported cases, the nature of the substrate curvature further dictates the tilt angle distribution of the lipids. Lipids in the convex region have a distribution peak that is close to that of a bilayer, and lipids in the flat and concave cases have their peaks at much higher angles. This finding shows that the effect of the substrate on the lipids is negligible in the convex region. The lipids in the flat and concave regions, however, are bent because of the substrate and exhibit higher tilt angles.

It should be noted that the slightly higher tilt angles of lipids in the concave region compared to those in the flat case may be a result of contributions from two factors: a greater adsorption degree and curvature of lipid tails induced because of the substrate (as the tails adsorb and line the curved graphene surface). Later, we will show using density profiles that there is in fact a greater degree of adsorption of lipid tails on concavely curved graphene compared to flat graphene.

Furthermore, the deviations in the tilt angle profiles between the three supported cases also depend on the substrate curvature. Coarse-grained simulations were performed for a larger wavelength graphene SLM system (see supporting information) and the results showed almost similar profiles for the concave and flat cases (Figure S3 (c)). However, there were still substantial deviations in the tilt angle profiles between convex and flat cases, although to a lesser extent.

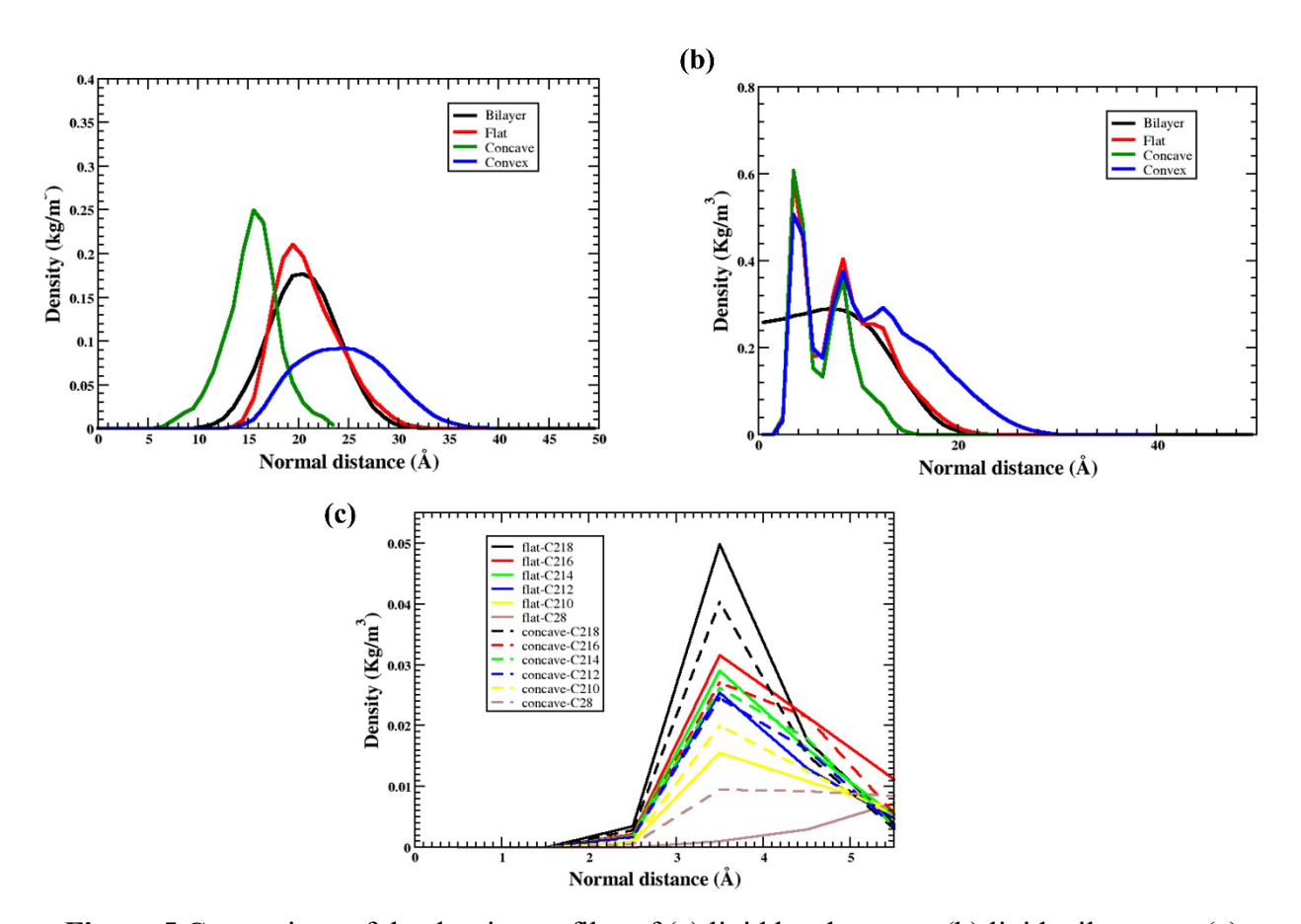


Figure 5 Comparison of the density profiles of (a) lipid head groups, (b) lipid tail groups, (c) individual carbon atoms, for the various systems considered in this study.

Density profiles- We computed the mass density profiles and compared them for lipids in the various cases considered in this study. To facilitate the comparison, we plotted separate figures for

the head groups (Figure 5(a)) and tail groups (Figure 5(b))) (see methods section for the classification details).

We observe a correlation in the trends from the previous sections on the order parameter and tilt angle with the trends observed in the density profile. First, the tail density profile plots show that there is greater adsorption of lipid tails in the concave region, followed by flat and convex surfaces. This discrepancy is evident from the first peak (closer to the substrate) of the tail density profiles, where the peak density values are almost the same for the concave and flat cases but lower for the convex case. It should be noted that because of the nature of the curvature, lipids in the concave region should have had a lower first peak value in the tail density and lipids in the convex region should have had a higher first peak value compared to the flat case⁶⁵. This is expected because when the lipid monolayer is concavely curved, the proximal tail carbons will have more volume to occupy, with the opposite expected in the convex case. However, for the first density peak values to exhibit the observed trend, the lipids in the concave region should be adsorbed to a greater degree compared to the flat case. To further validate this hypothesis, we computed the contributions of individual proximal carbons to the first peak density. Figure 5(c) shows that the contribution of the terminal carbons (C218, C216, and C214) to the first peak density in the flat case is higher than that in the concave case. However, the contribution of carbons more distant from graphene (C28 and C210) is higher in the concave case, which shows that the lipid tails are more bent in the concave case.

Furthermore, the head group density profiles show that the lipid head groups in the concave region are very tightly packed and those in the convex region are sparsely packed when compared to the flat case, which is again a result of the nature of the curvature. Another interesting physical change brought about by the substrate curvature is the thickness of the lipid monolayer. Based on

the positions of the peaks in the head group density profile, we can infer that the lipids in the concave region are compressed by \sim 4Å and lipids in the convex region are elongated by \sim 5Å compared to the flat case. These effects are not entirely due to the substrate because they have been observed in the case of curved bicelles in a previous study⁶⁵, although they were only observed in the concave case and to a much lesser extent (\sim 1.2 – 1.3Å). Similar to tilt angle profiles, density profiles also depend on the curvature of the substrate. For the larger wavelength SLM system, the deviations in head group and tail group density profiles (Figure S3 (a),(b)) between the three curvature cases show similar trends but less pronounced, compared to the smaller wavelength SLM system.

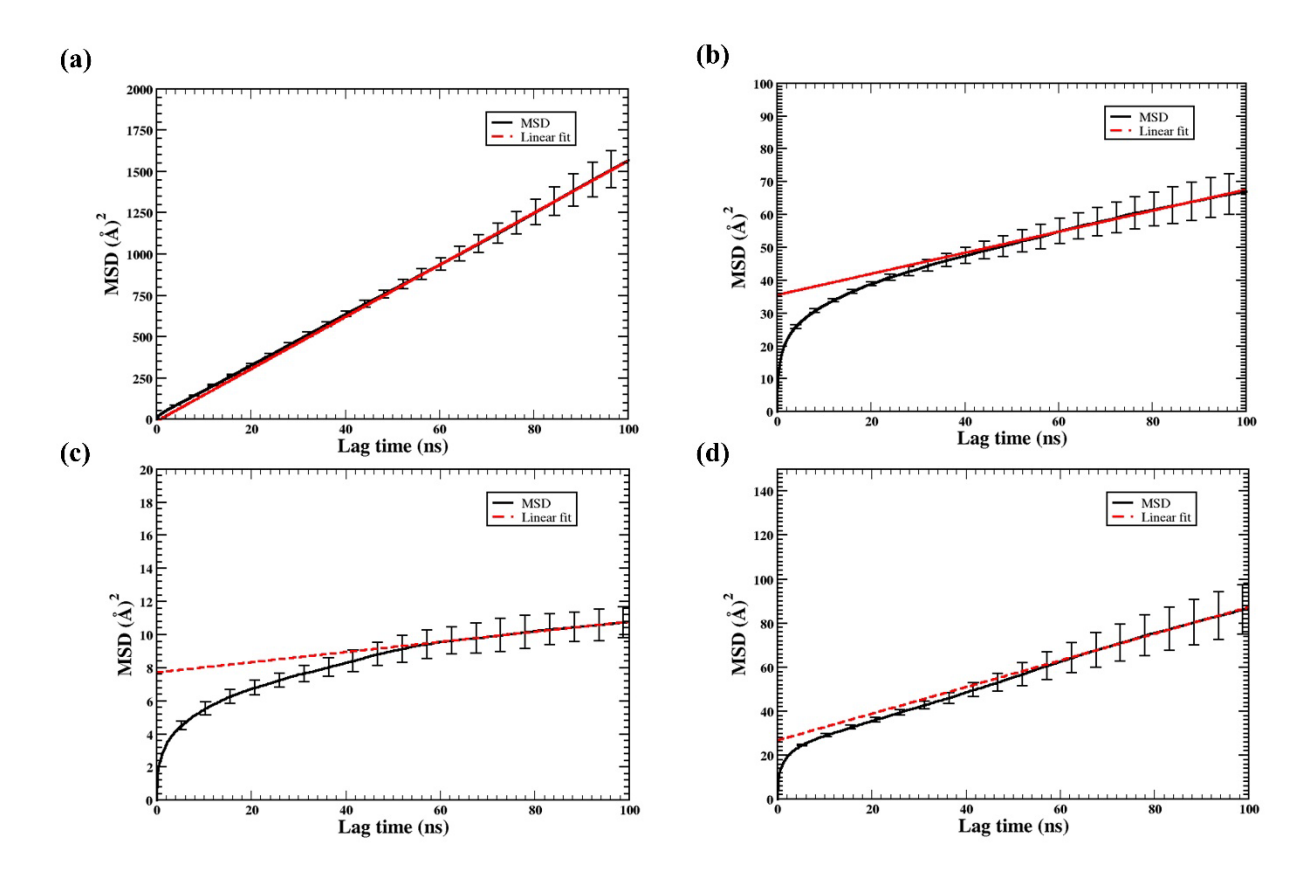


Figure 6 MSD plots for the various systems – (a) 2D MSD (x-y) for lipids in a bilayer, (b) 2D MSD (x-y) for lipids on a flat graphene substrate, (c) 1D MSD (y) for lipids on a concave graphene substrate, (d) 1D MSD (y) for lipids on a convex graphene substrate

Diffusion coefficient- To understand the changes in lipid dynamics caused by the substrate curvature, we computed the diffusion coefficient of the lipids in the various regions. The diffusion coefficient was computed from the slope of the long-time mean-squared diffusion profiles using Einstein's method (see methods section for the formulation). First, the presence of the substrate substantially reduces the diffusion coefficient of the lipids due to the adhesion of lipid tails to the graphene surface, which is evident from the lower diffusion coefficient values of supported lipids compared to a lipid bilayer reported in Table 1. This was also previously observed in lipid sesquilayers (1.5 bilayers) supported by graphene, where lipids directly adsorbed on graphene exhibited lower diffusion compared to the remaining bilayer⁶⁸.

Table 1 Diffusion coefficient values for lipids in the various systems considered in this study

System	Diffusion coefficient (μm²/s)
Bilayer	39.388 ± 5.06
Flat	0.76 ± 0.2
Concave	0.1631 ± 0.02
Convex	3.002 ± 0.54

Figure 6 and Table 1 also show that the nature of the substrate curvature further affects lipid diffusion, where lipids in the convex region diffuse the fastest among the supported lipid cases while lipids in the concave region diffuse the slowest. These results can be explained in terms of lipid graphene adhesion, where maximum adhesion is observed in the concave case and hence slower dynamics, and minimum adhesion is observed in the convex case and hence faster dynamics. It should be noted that, apart from the lipid-substrate adhesion, other factors could also be contributing to the observed trends in the lipid dynamics like packing and hydration⁶⁹. For

example, the higher head group packing density and lower hydration in the concave region, lower head group packing density and higher hydration in the convex region, could be contributing to the observed slower and faster dynamics in these regions, respectively.

CONCLUSIONS

In this work, we attempted to understand the structural and dynamical properties of lipids in the flat and deformed graphene SLMs. Our comparative study characterized the changes in the properties of lipid monolayers caused by the local nature of the substrate curvature supporting it. We observed that the concave nature of graphene enhances its lipophilic nature, which directly results in a greater extent of lipid tail adsorption. The opposite effect was observed in the case of convexly curved graphene. We learned that lipid tails are more ordered in the proximal part of the concave region and less ordered in the proximal part of the convex region compared to the flat case. We observed that the thickness of the lipid monolayer changed locally, with elongation observed in the convex case and compression observed in the concave case. We also learned that the lipid dynamics also changed, with lipids in the concave region diffusing more slowly and lipids in the convex region diffusing faster, compared to the flat case. The computational study presented here provides insights into how we can tailor the properties of lipids, such as the tail order, tail tilt, monolayer thickness, packing density, lateral diffusion rate and lipid-substrate interaction strength using the curvature of the supporting substrate. Such nanoscopic insights into the properties of supported lipids and the effect of curvature on these interfaces can help in the design of better biosensors and targeted drug-delivery systems.

SUPPORTING INFORMATION

Additional information about the construction of some simulated systems and CG benchmarking results.

ACKNOWLEDGMENTS

We gratefully acknowledge support from the National Science Foundation under grants 1720633 and 2140225. We acknowledge the use of the parallel computing resource Blue Waters provided by the University of Illinois and National Center for Supercomputing Applications.

REFERENCES

- (1) Raghunand, N.; Mahoney, B. P.; Gillies, R. J. Tumor Acidity, Ion Trapping and Chemotherapeutics: II. PH-Dependent Partition Coefficients Predict Importance of Ion Trapping on Pharmacokinetics of Weakly Basic Chemotherapeutic Agents. *Biochemical Pharmacology* **2003**, *66* (7), 1219–1229. https://doi.org/https://doi.org/10.1016/S0006-2952(03)00468-4.
- (2) Tan, S.; Tan, H. T.; Chung, M. C. M. Membrane Proteins and Membrane Proteomics. *PROTEOMICS* **2008**, *8* (19), 3924–3932. https://doi.org/https://doi.org/10.1002/pmic.200800597.
- (3) Lotvall, J.; Valadi, H. Cell to Cell Signalling via Exosomes Through EsRNA. *Cell Adhesion & Migration* **2007**, *I* (3), 156–158. https://doi.org/10.4161/cam.1.3.5114.
- (4) Hou, W.-C.; Moghadam, B. Y.; Corredor, C.; Westerhoff, P.; Posner, J. D. Distribution of Functionalized Gold Nanoparticles between Water and Lipid Bilayers as Model Cell Membranes. *Environmental Science & Technology* **2012**, *46* (3), 1869–1876. https://doi.org/10.1021/es203661k.
- (5) Dathe, M.; Meyer, J.; Beyermann, M.; Maul, B.; Hoischen, C.; Bienert, M. General Aspects of Peptide Selectivity towards Lipid Bilayers and Cell Membranes Studied by Variation of the Structural Parameters of Amphipathic Helical Model Peptides. *Biochimica et Biophysica Acta (BBA) Biomembranes* **2002**, *1558* (2), 171–186. https://doi.org/https://doi.org/10.1016/S0005-2736(01)00429-1.

- (6) Khandelia, H.; Duelund, L.; Pakkanen, K. I.; Ipsen, J. H. Triglyceride Blisters in Lipid Bilayers: Implications for Lipid Droplet Biogenesis and the Mobile Lipid Signal in Cancer Cell Membranes. *PLOS ONE* **2010**, *5* (9), e12811-.
- (7) MUELLER, P.; RUDIN, D. O.; TIEN, H. T. I.; WESCOTT, W. C. Reconstitution of Excitable Cell Membrane Structure in Vitro. *Circulation* **1962**, *26* (5), 1167–1171. https://doi.org/10.1161/01.CIR.26.5.1167.
- (8) JAIN, M. K.; STRICKHOLM, A.; CORDES, E. H. Reconstitution of an ATP-Mediated Active Transport System across Black Lipid Membranes. *Nature* **1969**, *222* (5196), 871–872. https://doi.org/10.1038/222871a0.
- (9) van Gelder, P.; Dumas, F.; Winterhalter, M. Understanding the Function of Bacterial Outer Membrane Channels by Reconstitution into Black Lipid Membranes. *Biophysical Chemistry* **2000**, *85* (2), 153–167. https://doi.org/https://doi.org/10.1016/S0301-4622(99)00153-2.
- (10) Winterhalter, M. Black Lipid Membranes. *Current Opinion in Colloid & Interface Science* **2000**, *5* (3), 250–255. https://doi.org/https://doi.org/10.1016/S1359-0294(00)00063-7.
- (11) Sebaaly, C.; Greige-Gerges, H.; Charcosset, C. Chapter 11 Lipid Membrane Models for Biomembrane Properties' Investigation. In *Current Trends and Future Developments on (Bio-) Membranes*; Basile, A., Charcosset, C., Eds.; Elsevier, 2019; pp 311–340. https://doi.org/https://doi.org/10.1016/B978-0-12-813606-5.00011-7.
- (12) McConnell, H. M.; Watts, T. H.; Weis, R. M.; Brian, A. A. Supported Planar Membranes in Studies of Cell-Cell Recognition in the Immune System. *Biochimica et Biophysica Acta (BBA) Reviews on Biomembranes* **1986**, *864* (1), 95–106. https://doi.org/https://doi.org/10.1016/0304-4157(86)90016-X.
- (13) Kiessling, V.; Domanska, M. K.; Murray, D.; Wan, C.; Tamm, L. K. Supported Lipid Bilayers. In *Wiley Encyclopedia of Chemical Biology*; John Wiley & Sons, Inc., 2008. https://doi.org/10.1002/9780470048672.wecb663.
- (14) Purrucker, O.; Hillebrandt, H.; Adlkofer, K.; Tanaka, M. Deposition of Highly Resistive Lipid Bilayer on Silicon–Silicon Dioxide Electrode and Incorporation of Gramicidin Studied by Ac Impedance Spectroscopy. *Electrochimica Acta* **2001**, *47* (5), 791–798. https://doi.org/https://doi.org/10.1016/S0013-4686(01)00759-9.
- (15) Mingeot-Leclercq, M.-P.; Deleu, M.; Brasseur, R.; Dufrêne, Y. F. Atomic Force Microscopy of Supported Lipid Bilayers. *Nature Protocols* **2008**, *3* (10), 1654–1659. https://doi.org/10.1038/nprot.2008.149.
- (16) Kraft, M. L.; Weber, P. K.; Longo, M. L.; Hutcheon, I. D.; Boxer, S. G. Phase Separation of Lipid Membranes Analyzed with High-Resolution Secondary Ion Mass Spectrometry. *Science* (1979) **2006**, 313 (5795), 1948. https://doi.org/10.1126/science.1130279.

- (17) Tamm, L. K.; Böhm, C.; Yang, J.; Shao, Z.; Hwang, J.; Edidin, M.; Betzig, E. Nanostructure of Supported Phospholipid Monolayers and Bilayers by Scanning Probe Microscopy. *Thin Solid Films* **1996**, *284*–*285*, 813–816. https://doi.org/https://doi.org/10.1016/S0040-6090(95)08453-3.
- (18) Ielasi, F. S.; Hirtz, M.; Sekula-Neuner, S.; Laue, T.; Fuchs, H.; Willaert, R. G. Dip-Pen Nanolithography-Assisted Protein Crystallization. *J Am Chem Soc* **2015**, *137* (1), 154–157. https://doi.org/10.1021/ja512141k.
- (19) Bog, U.; Laue, T.; Grossmann, T.; Beck, T.; Wienhold, T.; Richter, B.; Hirtz, M.; Fuchs, H.; Kalt, H.; Mappes, T. On-Chip Microlasers for Biomolecular Detection via Highly Localized Deposition of a Multifunctional Phospholipid Ink. *Lab on a Chip* **2013**, *13* (14), 2701–2707. https://doi.org/10.1039/C3LC50149C.
- (20) Kuo, C.-J.; Chiang, H.-C.; Tseng, C.-A.; Chang, C.-F.; Ulaganathan, R. K.; Ling, T.-T.; Chang, Y.-J.; Chen, C.-C.; Chen, Y.-R.; Chen, Y.-T. Lipid-Modified Graphene-Transistor Biosensor for Monitoring Amyloid-β Aggregation. *ACS Applied Materials & Interfaces* **2018**, *10* (15), 12311–12316. https://doi.org/10.1021/acsami.8b01917.
- (21) Ang, P. K.; Jaiswal, M.; Lim, C. H. Y. X.; Wang, Y.; Sankaran, J.; Li, A.; Lim, C. T.; Wohland, T.; Barbaros, Ö.; Loh, K. P. A Bioelectronic Platform Using a Graphene–Lipid Bilayer Interface. *ACS Nano* **2010**, *4* (12), 7387–7394. https://doi.org/10.1021/nn1022582.
- (22) Kang, J. H.; Ko, Y. T. Lipid-Coated Gold Nanocomposites for Enhanced Cancer Therapy. *Int J Nanomedicine* **2015**, *10 Spec Iss* (Spec Iss), 33–45. https://doi.org/10.2147/IJN.S88307.
- (23) Ashley, C. E.; Carnes, E. C.; Phillips, G. K.; Padilla, D.; Durfee, P. N.; Brown, P. A.; Hanna, T. N.; Liu, J.; Phillips, B.; Carter, M. B.; Carroll, N. J.; Jiang, X.; Dunphy, D. R.; Willman, C. L.; Petsev, D. N.; Evans, D. G.; Parikh, A. N.; Chackerian, B.; Wharton, W.; Peabody, D. S.; Brinker, C. J. The Targeted Delivery of Multicomponent Cargos to Cancer Cells by Nanoporous Particle-Supported Lipid Bilayers. *Nature Materials* **2011**, *10* (5), 389–397. https://doi.org/10.1038/nmat2992.
- (24) Nikoleli, G.-P.; Siontorou, C.; Nikolelis, D.; Bratakou, S.; Karapetis, S.; Tzamtzis, N. Biosensors Based on Lipid Modified Graphene Microelectrodes. *C (Basel)* **2017**, *3* (4), 9. https://doi.org/10.3390/c3010009.
- (25) Imran, H.; Manikandan, P. N.; Dharuman, V. Graphene Oxide Supported Liposomes for Efficient Label Free Electrochemical DNA Biosensing. *Sensors and Actuators B: Chemical* **2018**, *260*, 841–851. https://doi.org/https://doi.org/10.1016/j.snb.2018.01.103.
- (26) Blaschke, B. M.; Böhm, P.; Drieschner, S.; Nickel, B.; Garrido, J. A. Lipid Monolayer Formation and Lipid Exchange Monitored by a Graphene Field-Effect Transistor. *Langmuir* **2018**, *34* (14), 4224–4233. https://doi.org/10.1021/acs.langmuir.8b00162.

- (27) Poursoroush, A.; Sperotto, M. M.; Laradji, M. Phase Behavior of Supported Lipid Bilayers: A Systematic Study by Coarse-Grained Molecular Dynamics Simulations. *The Journal of Chemical Physics* **2017**, *146* (15), 154902. https://doi.org/10.1063/1.4981008.
- (28) Xing, C.; Faller, R. Density Imbalances and Free Energy of Lipid Transfer in Supported Lipid Bilayers. *The Journal of Chemical Physics* **2009**, *131* (17), 175104. https://doi.org/10.1063/1.3262315.
- (29) Rivel, T.; Yesylevskyy, S. O.; Ramseyer, C. Structures of Single, Double and Triple Layers of Lipids Adsorbed on Graphene: Insights from All-Atom Molecular Dynamics Simulations. *Carbon N Y* 2017, 118, 358–369. https://doi.org/https://doi.org/10.1016/j.carbon.2017.03.072.
- (30) Willems, N.; Urtizberea, A.; Verre, A. F.; Iliut, M.; Lelimousin, M.; Hirtz, M.; Vijayaraghavan, A.; Sansom, M. S. P. Biomimetic Phospholipid Membrane Organization on Graphene and Graphene Oxide Surfaces: A Molecular Dynamics Simulation Study. *ACS Nano* 2017, 11 (2), 1613–1625. https://doi.org/10.1021/acsnano.6b07352.
- (31) Nicholl, R. J. T.; Conley, H. J.; Lavrik, N. v; Vlassiouk, I.; Puzyrev, Y. S.; Sreenivas, V. P.; Pantelides, S. T.; Bolotin, K. I. The Effect of Intrinsic Crumpling on the Mechanics of Free-Standing Graphene. *Nature Communications* **2015**, *6* (1), 8789. https://doi.org/10.1038/ncomms9789.
- (32) Tripathi, M.; Lee, F.; Michail, A.; Anestopoulos, D.; McHugh, J. G.; Ogilvie, S. P.; Large, M. J.; Graf, A. A.; Lynch, P. J.; Parthenios, J.; Papagelis, K.; Roy, S.; Saadi, M. A. S. R.; Rahman, M. M.; Pugno, N. M.; King, A. A. K.; Ajayan, P. M.; Dalton, A. B. Structural Defects Modulate Electronic and Nanomechanical Properties of 2D Materials. ACS Nano 2021, 15 (2), 2520–2531. https://doi.org/10.1021/acsnano.0c06701.
- (33) Hwang, M. T.; Heiranian, M.; Kim, Y.; You, S.; Leem, J.; Taqieddin, A.; Faramarzi, V.; Jing, Y.; Park, I.; van der Zande, A. M.; Nam, S.; Aluru, N. R.; Bashir, R. Ultrasensitive Detection of Nucleic Acids Using Deformed Graphene Channel Field Effect Biosensors. *Nature Communications* **2020**, *11* (1), 1543. https://doi.org/10.1038/s41467-020-15330-9.
- (34) Huang, J.; Rauscher, S.; Nawrocki, G.; Ran, T.; Feig, M.; de Groot, B. L.; Grubmüller, H.; MacKerell, A. D. CHARMM36m: An Improved Force Field for Folded and Intrinsically Disordered Proteins. *Nature Methods* **2017**, *14* (1), 71–73. https://doi.org/10.1038/nmeth.4067.
- (35) Toda, M.; Kubo, R.; Saitō, N.; Hashitsume, N. *Statistical Physics II: Nonequilibrium Statistical Mechanics*; Springer Science & Business Media, 1991; Vol. 2.
- (36) Brünger, A.; Brooks, C. L.; Karplus, M. Stochastic Boundary Conditions for Molecular Dynamics Simulations of ST2 Water. *Chemical Physics Letters* **1984**, *105* (5), 495–500. https://doi.org/https://doi.org/10.1016/0009-2614(84)80098-6.

- (37) Martyna, G. J.; Tobias, D. J.; Klein, M. L. Constant Pressure Molecular Dynamics Algorithms. *The Journal of Chemical Physics* **1994**, *101* (5), 4177–4189. https://doi.org/10.1063/1.467468.
- (38) Feller, S. E.; Zhang, Y.; Pastor, R. W.; Brooks, B. R. Constant Pressure Molecular Dynamics Simulation: The Langevin Piston Method. *The Journal of Chemical Physics* **1995**, *103* (11), 4613–4621. https://doi.org/10.1063/1.470648.
- (39) Darden, T.; York, D.; Pedersen, L. Particle Mesh Ewald: An N·log(N) Method for Ewald Sums in Large Systems. *The Journal of Chemical Physics* **1993**, *98* (12), 10089–10092. https://doi.org/10.1063/1.464397.
- (40) Phillips, J. C.; Braun, R.; Wang, W.; Gumbart, J.; Tajkhorshid, E.; Villa, E.; Chipot, C.; Skeel, R. D.; Kalé, L.; Schulten, K. Scalable Molecular Dynamics with NAMD. *Journal of Computational Chemistry* **2005**, *26* (16), 1781–1802. https://doi.org/https://doi.org/10.1002/jcc.20289.
- (41) Jorgensen, W. L.; Chandrasekhar, J.; Madura, J. D.; Impey, R. W.; Klein, M. L. Comparison of Simple Potential Functions for Simulating Liquid Water. *The Journal of Chemical Physics* **1983**, *79* (2), 926–935. https://doi.org/10.1063/1.445869.
- (42) Humphrey, W.; Dalke, A.; Schulten, K. VMD: Visual Molecular Dynamics. *Journal of Molecular Graphics* **1996**, *14* (1), 33–38. https://doi.org/https://doi.org/10.1016/0263-7855(96)00018-5.
- (43) Lima, L. M. C.; Fu, W.; Jiang, L.; Kros, A.; Schneider, G. F. Graphene-Stabilized Lipid Monolayer Heterostructures: A Novel Biomembrane Superstructure. *Nanoscale* **2016**, *8* (44), 18646–18653. https://doi.org/10.1039/C6NR05706C.
- (44) Rui, L.; Liu, J.; Li, J.; Weng, Y.; Dou, Y.; Yuan, B.; Yang, K.; Ma, Y. Reduced Graphene Oxide Directed Self-Assembly of Phospholipid Monolayers in Liquid and Gel Phases. *Biochimica et Biophysica Acta (BBA) Biomembranes* **2015**, *1848* (5), 1203–1211. https://doi.org/https://doi.org/10.1016/j.bbamem.2015.02.018.
- (45) Yu, Z.-W.; Jin, J.; Cao, Y. Characterization of the Liquid-Expanded to Liquid-Condensed Phase Transition of Monolayers by Means of Compressibility. *Langmuir* **2002**, *18* (11), 4530–4531. https://doi.org/10.1021/la011840+.
- (46) Xing, C.; Faller, R. Interactions of Lipid Bilayers with Supports: A Coarse-Grained Molecular Simulation Study. *The Journal of Physical Chemistry B* **2008**, *112* (23), 7086–7094. https://doi.org/10.1021/jp0773051.
- (47) Kaznessis, Y. N.; Kim, S.; Larson, R. G. Simulations of Zwitterionic and Anionic Phospholipid Monolayers. *Biophysical Journal* **2002**, *82* (4), 1731–1742. https://doi.org/https://doi.org/10.1016/S0006-3495(02)75525-2.
- (48) Vermeer, L. S.; de Groot, B. L.; Réat, V.; Milon, A.; Czaplicki, J. Acyl Chain Order Parameter Profiles in Phospholipid Bilayers: Computation from Molecular Dynamics

- Simulations and Comparison with 2 H NMR Experiments. *European Biophysics Journal* **2007**, *36* (8), 919–931.
- (49) Johner, N.; Harries, D.; Khelashvili, G. Implementation of a Methodology for Determining Elastic Properties of Lipid Assemblies from Molecular Dynamics Simulations. *BMC Bioinformatics* **2016**, *17* (1), 161. https://doi.org/10.1186/s12859-016-1003-z.
- (50) Khan, H. M.; Souza, P. C. T.; Thallmair, S.; Barnoud, J.; de Vries, A. H.; Marrink, S. J.; Reuter, N. Capturing Choline–Aromatics Cation–π Interactions in the MARTINI Force Field. *Journal of Chemical Theory and Computation* **2020**, *16* (4), 2550–2560. https://doi.org/10.1021/acs.jctc.9b01194.
- (51) de Jong, D. H.; Singh, G.; Bennett, W. F. D.; Arnarez, C.; Wassenaar, T. A.; Schäfer, L. v; Periole, X.; Tieleman, D. P.; Marrink, S. J. Improved Parameters for the Martini Coarse-Grained Protein Force Field. *Journal of Chemical Theory and Computation* **2013**, *9* (1), 687–697. https://doi.org/10.1021/ct300646g.
- (52) Yesylevskyy, S. O.; Schäfer, L. v; Sengupta, D.; Marrink, S. J. Polarizable Water Model for the Coarse-Grained MARTINI Force Field. *PLOS Computational Biology* **2010**, *6* (6), e1000810-.
- (53) Berendsen, H. J. C.; van der Spoel, D.; van Drunen, R. GROMACS: A Message-Passing Parallel Molecular Dynamics Implementation. *Computer Physics Communications* **1995**, *91* (1), 43–56. https://doi.org/https://doi.org/10.1016/0010-4655(95)00042-E.
- (54) Hess, B.; Kutzner, C.; van der Spoel, D.; Lindahl, E. GROMACS 4: Algorithms for Highly Efficient, Load-Balanced, and Scalable Molecular Simulation. *Journal of Chemical Theory and Computation* **2008**, *4* (3), 435–447. https://doi.org/10.1021/ct700301q.
- (55) Pronk, S.; Páll, S.; Schulz, R.; Larsson, P.; Bjelkmar, P.; Apostolov, R.; Shirts, M. R.; Smith, J. C.; Kasson, P. M.; van der Spoel, D.; Hess, B.; Lindahl, E. GROMACS 4.5: A High-Throughput and Highly Parallel Open Source Molecular Simulation Toolkit. *Bioinformatics* **2013**, *29* (7), 845–854. https://doi.org/10.1093/bioinformatics/btt055.
- (56) Páll, S.; Abraham, M. J.; Kutzner, C.; Hess, B.; Lindahl, E. Tackling Exascale Software Challenges in Molecular Dynamics Simulations with GROMACS. In *Solving Software Challenges for Exascale*; Markidis, S., Laure, E., Eds.; Springer International Publishing: Cham, 2015; pp 3–27.
- (57) Abraham, M. J.; Murtola, T.; Schulz, R.; Páll, S.; Smith, J. C.; Hess, B.; Lindahl, E. GROMACS: High Performance Molecular Simulations through Multi-Level Parallelism from Laptops to Supercomputers. *SoftwareX* **2015**, *1*–2, 19–25. https://doi.org/https://doi.org/10.1016/j.softx.2015.06.001.

- (58) Yesylevskyy, S. O.; Schäfer, L. v; Sengupta, D.; Marrink, S. J. Polarizable Water Model for the Coarse-Grained MARTINI Force Field. *PLOS Computational Biology* **2010**, *6* (6), e1000810-.
- (59) Bussi, G.; Zykova-Timan, T.; Parrinello, M. Isothermal-Isobaric Molecular Dynamics Using Stochastic Velocity Rescaling. *The Journal of Chemical Physics* **2009**, *130* (7), 074101. https://doi.org/10.1063/1.3073889.
- (60) Parrinello, M.; Rahman, A. Polymorphic Transitions in Single Crystals: A New Molecular Dynamics Method. *Journal of Applied Physics* **1981**, *52* (12), 7182–7190. https://doi.org/10.1063/1.328693.
- (61) Bemporad, D.; Essex, J. W.; Luttmann, C. Permeation of Small Molecules through a Lipid Bilayer: A Computer Simulation Study. *The Journal of Physical Chemistry B* **2004**, *108* (15), 4875–4884. https://doi.org/10.1021/jp035260s.
- (62) Bennett, W. F. D.; Tieleman, D. P. Computer Simulations of Lipid Membrane Domains. *Biochimica et Biophysica Acta (BBA) Biomembranes* **2013**, *1828* (8), 1765–1776. https://doi.org/https://doi.org/10.1016/j.bbamem.2013.03.004.
- (63) Jan Akhunzada, M.; D'Autilia, F.; Chandramouli, B.; Bhattacharjee, N.; Catte, A.; di Rienzo, R.; Cardarelli, F.; Brancato, G. Interplay between Lipid Lateral Diffusion, Dye Concentration and Membrane Permeability Unveiled by a Combined Spectroscopic and Computational Study of a Model Lipid Bilayer. *Scientific Reports* **2019**, *9* (1), 1508. https://doi.org/10.1038/s41598-018-37814-x.
- (64) Einstein, A. On the Movement of Small Particles Suspended in Stationary Liquids Required by the Molecularkinetic Theory of Heat. *Ann. d. Phys* **1905**, *17* (549–560), 1.
- (65) Yesylevskyy, S. O.; Rivel, T.; Ramseyer, C. The Influence of Curvature on the Properties of the Plasma Membrane. Insights from Atomistic Molecular Dynamics Simulations. *Scientific Reports* **2017**, *7* (1), 16078. https://doi.org/10.1038/s41598-017-16450-x.
- (66) Hwang, M. T.; Heiranian, M.; Kim, Y.; You, S.; Leem, J.; Taqieddin, A.; Faramarzi, V.; Jing, Y.; Park, I.; van der Zande, A. M.; Nam, S.; Aluru, N. R.; Bashir, R. Ultrasensitive Detection of Nucleic Acids Using Deformed Graphene Channel Field Effect Biosensors. *Nature Communications* 2020, 11 (1), 1543. https://doi.org/10.1038/s41467-020-15330-9.
- (67) Lee, J.-K.; Yamazaki, S.; Yun, H.; Park, J.; Kennedy, G. P.; Kim, G.-T.; Pietzsch, O.; Wiesendanger, R.; Lee, S.; Hong, S.; Dettlaff-Weglikowska, U.; Roth, S. Modification of Electrical Properties of Graphene by Substrate-Induced Nanomodulation. *Nano Letters* **2013**, *13* (8), 3494–3500. https://doi.org/10.1021/nl400827p.
- (68) Farell, M.; Wetherington, M.; Shankla, M.; Chae, I.; Subramanian, S.; Kim, S. H.; Aksimentiev, A.; Robinson, J.; Kumar, M. Characterization of the Lipid Structure and Fluidity of Lipid Membranes on Epitaxial Graphene and Their Correlation to Graphene Features. *Langmuir* 2019, 35 (13), 4726–4735. https://doi.org/10.1021/acs.langmuir.9b00164.

(69) Hirtz, M.; Oikonomou, A.; Georgiou, T.; Fuchs, H.; Vijayaraghavan, A. Multiplexed Biomimetic Lipid Membranes on Graphene by Dip-Pen Nanolithography. *Nature Communications* **2013**, *4* (1), 2591. https://doi.org/10.1038/ncomms3591.

FOR TABLE OF CONTENTS ONLY

